



Efficient and selective removal of Pb(II) from landfill leachate using L-serine-modified polyethylene/polypropylene nonwoven fabric synthesized via radiation grafting technique

Xin-Xin Feng^{1,2} · Cheng Li¹ · Xuan-Zhi Mao^{1,2} · Wan-Ning Ren^{1,3} · Yang Gao^{1,2} · Yu-Long He^{1,2} · Zhe Xing¹ · Rong Li¹ · Guo-Zhong Wu^{1,3}

Received: 9 June 2023 / Revised: 30 November 2023 / Accepted: 14 December 2023 / Published online: 24 May 2024

© The Author(s), under exclusive licence to China Science Publishing & Media Ltd. (Science Press), Shanghai Institute of Applied Physics, the Chinese Academy of Sciences, Chinese Nuclear Society 2024

Abstract

In this study, to efficiently remove Pb(II) from aqueous environments, a novel L-serine-modified polyethylene/polypropylene nonwoven fabric sorbent (NWF-serine) was fabricated through the radiation grafting of glycidyl methacrylate and subsequent L-serine modification. The effect of the absorbed dose was investigated in the range of 5–50 kGy. NWF-serine was characterized by Fourier transform infrared spectroscopy, thermogravimetric analysis, and scanning electron microscopy. Batch adsorption tests were conducted to investigate the influences of pH, adsorption time, temperature, initial concentration, and sorbent dosage on the Pb(II) adsorption performance of NWF-serine. The results indicated that Pb(II) adsorption onto NWF-serine was an endothermic process, following the pseudo-second-order kinetic model and Langmuir isotherm model. The saturated adsorption capacity was 198.1 mg/g. NWF-serine exhibited Pb(II) removal rates of 99.8% for aqueous solutions with initial concentrations of 100 mg/L and 82.1% for landfill leachate containing competitive metal ions such as Cd, Cu, Ni, Mn, and Zn. Furthermore, NWF-serine maintained 86% of its Pb(II) uptake after five use cycles. The coordination of the carboxyl and amino groups with Pb(II) was confirmed using X-ray photoelectron spectroscopy and extended X-ray absorption fine structure analysis.

Keywords Landfill leachate · Radiation grafting · Polyethylene/polypropylene nonwoven fabric · Pb(II) removal

1 Introduction

Currently, sanitary landfilling is an economical and easy strategy that is applied to approximately 95% of the total municipal solid waste collected worldwide [1]. However,

the leachate that percolate through waste deposits contain numerous organic, inorganic, ammonium, and toxic constituents, resulting in severe long-term soil and groundwater contamination [1, 2]. Lead (Pb) is a typical toxic heavy metal present in landfill leachate. It is non-degradable, bioaccumulative, and biologically toxic, thus posing a potential threat to human health and ecosystems. Excessive Pb exposure can cause cardiovascular, neurological, and renal disorders [3]. Furthermore, Pb exposure adversely affects plant and animal growth [4]. The World Health Organization (WHO) and China (GB 16889-2008) have proposed the maximum permissible concentrations for Pb in drinking water (0.01 mg/L) and discharged landfill leachate (0.1 mg/L), respectively [5, 6]. Therefore, the removal of Pb contaminants from landfill leachates is indispensable.

Adsorption is an attractive method for removing heavy-metal ions from aqueous environments and offers advantages such as ease of operation, low cost, and high efficiency [7]. Various sorbents for heavy-metal ions have been reported,

This work was supported by the National Natural Science Foundation of China (Nos. 11605275 and 11675247).

✉ Rong Li
lirong@sinap.ac.cn

✉ Guo-Zhong Wu
wuguozhong@sinap.ac.cn

¹ Shanghai Institute of Applied Physics, Chinese Academy of Sciences, Shanghai 201800, China

² University of Chinese Academy of Sciences, Beijing 100049, China

³ School of Physical Science and Technology, ShanghaiTech University, Shanghai 201210, China

including carbon nanotubes, zeolites, covalent organic frameworks, microorganisms, and polymer sorbents [8–11]. In chemical adsorption, the binding between the sorbents and heavy-metal ions relies on the formation of chemical bonds. Consequently, sorbent modifications often select groups with electric charges and atoms with lone pairs of electrons. For example, phosphoric acid-modified hydrochar exhibited a Pb(II) uptake of 353.4 mg/g, which is approximately 10 times that of an unmodified sample [12]. The reported polyacrylonitrile beads exhibited a Pb(II) uptake of 145 mg/g, with the carboxyl and amino groups generated through nitrile rearrangement after NaOH treatment as the active sites [13]. Compared with powdered or granular sorbents, functional sorbents based on polymer fibers or fabrics can be easily deployed and recycled [14], avoiding the problem of easy loss during usage.

Serine, a natural amino acid, contains amino, hydroxyl, and carboxyl groups that provide active binding sites for heavy-metal ions. Sorbents based on serine or its derivatives have been synthesized to detect or remove heavy-metal ions such as lead (serine diacetic acid-modified chelating resin) [15] and uranium (serine-derived chitosan resin) [16]. Furthermore, typical positively charged dyes, such as rhodamine B (L-serine-capped magnetite nanoparticles) [17] and malachite green [poly (N-acryloyl-L-serine) grafted-kaolin] [18] can also be efficiently removed. In addition, serine is nontoxic and accessible as a raw material. To the best of our knowledge, the use of serine-modified nonwoven fabric sorbents for the removal of toxic heavy-metal ions has not yet been reported.

Radiation grafting is an efficient technique for introducing the desired functional groups into various polymer substrates in the shape of films, membranes, and fibers [19]. Using high-energy rays such as electron beams and gamma rays, free radicals can be easily generated in polymers at room temperature without chemical reagents. The polyethylene/polypropylene skin-core nonwoven fabric (PE/PP NWF) used in this work consists of fibers with a diameter of 10 μm , in which PE forms the skin layer and PP comprises the inner core. The synergistic properties of these two components result in a lightweight, thin, and soft fabric that is well-suited for the preparation of sorbents.

The complex composition of landfill leachate (high salinity, multiple coexisting metal ions, and large amounts of organic matter) requires sorbents with high adsorption capacity and selectivity. In this study, an L-serine-modified PE/PP NWF (NWF-serine) was conveniently synthesized via the radiation grafting of glycidyl methacrylate (GMA), followed by a ring-opening reaction with L-serine. The Pb(II) adsorption performance of NWF-serine was evaluated through batch adsorption tests in aqueous solutions and landfill leachate.

2 Experimental section

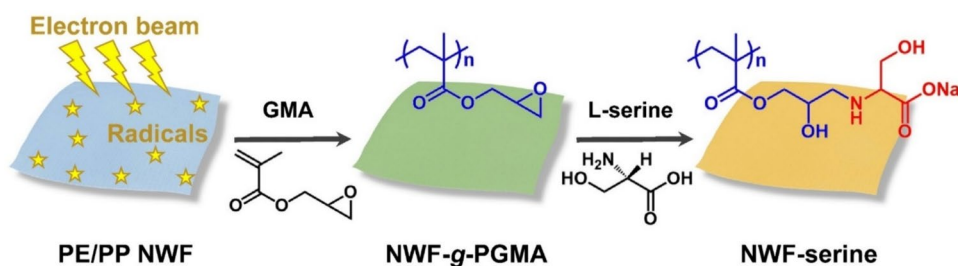
2.1 Materials

The PE/PP NWF was obtained from Henan Kegao Radiation Chemical Technology Co., Ltd. L-serine, lead chloride (PbCl_2 , 99.99% metal basis), and 1, 4-dioxane were purchased from Shanghai Macklin Biochemical Co., Ltd. Glycidyl methacrylate (GMA) was purchased from Sigma-Aldrich (Shanghai) Trading Co., Ltd. Hydrochloric acid, methanol, and sodium hydroxide were supplied by Sinopharm Chemical Reagent Co., Ltd. All the reagents were of analytical grade and were used without further refinement.

2.2 Synthesis of NWF-serine

The synthetic procedure for the NWF-serine sorbent is shown in Fig. 1. First, the PE/PP NWF were irradiated at different absorbed doses using an electron-beam accelerator (Shanghai Institute of Applied Physics). Subsequently, 2 g of the irradiated NWF substrate was transferred to a conical flask containing 10 mL GMA, 95 mL methanol, and 95 mL H_2O . The grafting reaction was performed at 65 $^\circ\text{C}$ for 3 h and was protected using nitrogen gas [14]. The grafted samples (denoted as NWF-g-PGMA) were rinsed with methanol and distilled water to remove the unreacted monomers and residual homopolymers. Subsequently, NWF-g-PGMA was dried under vacuum overnight at 60 $^\circ\text{C}$. The degree of grafting (D_g) of the NWF-g-PGMA was calculated using Eq. (1), as follows.

Fig. 1 Synthetic route of the NWF-serine sorbent



$$D_g(\%) = \frac{W_1 - W_0}{W_0} \times 100 \quad (1)$$

where W_0 (g) and W_1 (g) are the weights of the NWF samples before and after the grafting, respectively. To prepare the solution for subsequent modification, 5 g of L-serine was dissolved in 50 mL of distilled water and the pH was adjusted to 9 using NaOH. Subsequently, 50 mL of 1,4-dioxane was added to the L-serine solution and mixed evenly. Next, 3 g of NWF-*g*-PGMA was submerged into the L-serine solution, and the reaction was maintained at 80 °C for 24 h. The serine-modified sample (coded as NWF-serine) was washed with methanol and distilled water to remove unreacted L-serine and residual solvents and then dried overnight at 60 °C. The density of the L-serine units and conversion rate of the epoxy groups were quantified using Eqs. (2) and (3), respectively. To mitigate the influence of the Na element on the calculation, the NWF-serine was immersed in 0.5 mol/L HCl solution for 1 h, rinsed with distilled water, and dried at 60 °C.

$$L - \text{serine unit density}(\text{mmol/g}) = \frac{W_2 - W_1}{105.1 \times W_2} \times 1000 \quad (2)$$

$$\text{Conversion rate of epoxy group}(\%) = \frac{(W_2 - W_1) \times 142.2}{(W_1 - W_0) \times 105.1} \times 100 \quad (3)$$

where W_1 (g) and W_2 (g) are the weights of the NWF samples before and after the L-serine modification, respectively; 105.1 and 142.2 are the molecule weights of L-serine and GMA, respectively. In the NWF-serine used for subsequent adsorption, the obtained results were as follows: D_g of 244%, an L-serine unit density of 2.2 mmol/g, and an epoxy groups conversion rate of 59%.

2.3 Characterization

An electron spin resonance (ESR) spectrometer (JEOL JES-FA200) was used to collect the free radical signals of the irradiated PE/PP NWF samples. The ESR tests were conducted in air with a center frequency of 9.1 GHz, power of 1 mW, and nuclear magnetic frequency modulation of 100 kHz. The Fourier transformed infrared (FTIR; Bruker Tensor 27) spectra of the modified samples were collected by performing 32 automatic scans in the range of 600–4000 cm^{-1} with a wavenumber resolution of 4 cm^{-1} . The thermogravimetric analyses (TGA; NETZSCH 209 F3) of the samples were conducted under a nitrogen atmosphere (temperature: 30–600 °C; heating velocity: 10 °C/min). The derivative thermogravimetry (DTG) results were obtained by the first derivative of the TGA results. Scanning electron microscopy (SEM; Zeiss Merlin Compact) was used

to distinguish the micromorphological changes in the pristine, modified, and Pb-loaded (coded as Pb@NWF-serine) samples. Energy-dispersive spectroscopy (EDS) was used to analyze the elemental composition and distribution of NWF-serine and Pb@NWF-serine at an acceleration voltage of 20 kV. The X-ray photoelectron spectroscopy (XPS; Thermo Scientific Escalab 250Xi) patterns of the NWF-serine and Pb@NWF-serine were acquired under Al $K\alpha$ radiation. X-ray absorption fine structure (EXAFS) data for Pb@NWF-serine were collected at the Pb L3 edge (13,035 eV) with fluorescence geometry at the Shanghai Synchrotron Radiation Facility (BL14W1 beamline). Self-absorption effects were corrected before analysis. ATHENA and ARTEMIS were used to analyze the collected EXAFS data [20].

2.4 Adsorption tests

A Pb(II) stock solution (200 mg/L) was prepared in a volumetric flask using PbCl_2 and diluted to different concentrations for the subsequent sorption tests. The prepared Pb(II) solutions were placed in plastic bottles, and all adsorption tests were performed using an oscillator at a rotation rate of 100 rpm. Different variables, including the initial pH, sorption time, temperature, initial Pb(II) concentration, NWF-serine dosage, and number of reuses, were investigated via batch adsorption tests. Additionally, landfill leachate containing heavy-metal ions was used to evaluate the adsorption performance of NWF-serine. The metal ion concentrations were determined using inductively coupled plasma optical emission spectrometry (ICP-OES; PerkinElmer Optima 8000) and inductively coupled plasma-mass spectrometry (ICP-MS; PerkinElmer NexION 300 D). The adsorption amount (Q , mg/g) and removal rate of metal ions were determined using Eqs. (4) and (5), respectively.

$$Q = \frac{(C_0 - C_1) \times V}{W_3} \quad (4)$$

$$\text{Removal rate}(\%) = \frac{C_0 - C_1}{C_0} \times 100 \quad (5)$$

where C_0 (mg/L) and C_1 (mg/L) are the concentrations of the metal ions before and after adsorption, respectively; V (L) is the volume of the solution, and W_3 (g) is the weight of the NWF-serine sorbent.

3 Results and discussion

3.1 Influence of absorbed dose

Radiation-initiated polymerization uses high-energy rays to generate free radicals uniformly on polymer substrates,

which can initiate the graft polymerization of vinyl monomers. In this study, the paramagnetic substances and intermediates present in the irradiated PE/PP NWF were characterized by ESR tests. As shown in Fig. 2a, the ESR signal intensity increases as the absorbed dose increases from 0 to 50 kGy, indicating an increase in the concentration of free radicals. During the initial polymerization stage, the primary free radicals were terminated either by inhibitors or residual oxygen present in the unpurified monomer solution, resulting in a low D_g (69.3%) at 5 kGy (Fig. 2b). Increasing the absorbed dose significantly enhanced the D_g of GMA, which is primarily attributed to the increasing number of free radicals serving as active sites for graft polymerization. In addition to the primary free radicals, peroxides generated during irradiation can decompose into free radicals upon heating during polymerization [21]. A high D_g (406%) was achieved at an absorbed dose of 50 kGy with a good GMA conversion ratio of 81%. However, both the high absorbed dose and the D_g of GMA can lead to a sharp deterioration in the mechanical properties of the polymer substrate. Hence, an absorbed dose of 20 kGy was selected for sorbent synthesis.

3.2 Structural characterization

3.2.1 FTIR

FTIR spectroscopy was used to characterize the chemical compositions of the NWF samples (Fig. 3a). Four characteristic peaks were discernible in the spectrum of the PE/PP NWF, ascribed to asymmetric stretching (2914 cm^{-1}), symmetric stretching (2849 cm^{-1}), asymmetric bending (1472 cm^{-1}), and in-plane deformation rocking (717 cm^{-1}) of the $-\text{CH}_2-$ units in PE molecular chains [22]. After the introduction of the PGMA chains, the emerging peaks were consistent with CH_3 stretching (3001 cm^{-1}), $\text{C}=\text{O}$ stretching (1724 cm^{-1}), $\text{C}-\text{O}-\text{C}$ stretching (1146 cm^{-1}), and

epoxy groups (843 cm^{-1}) [23]. After the L-serine modification, the disappearance of the peak corresponding to the epoxy groups and the emergence of peaks corresponding to $\text{O}-\text{H}/\text{N}-\text{H}$ ($3680-3040\text{ cm}^{-1}$) and $\text{C}=\text{O}$ (1568 cm^{-1} , belonging to $-\text{COO}^-$) indicate a successful reaction between the epoxy groups and L-serine.

3.2.2 TGA and DTG

TGA analysis was conducted to investigate the thermal stability of the pristine and modified NWF samples (Fig. 3b, c). The pristine PE/PP NWF exhibited only one thermal degradation platform with an initial decomposition temperature (where a mass loss of 5% occurred) of $410\text{ }^\circ\text{C}$. After grafting, the NWF-*g*-PGMA sample exhibited two extra thermal degradation platforms with maximum degradation rates at 229 and $340\text{ }^\circ\text{C}$, ascribed to the degradation of oxygen-containing groups and graft chains, respectively [24]. After the introduction of L-serine, a more complex thermal degradation behavior was observed. The thermal decomposition platform between 30 and $137\text{ }^\circ\text{C}$ was assigned to the evaporation of moisture and volatile substances. Compared to NWF-*g*-PGMA, the initial thermal degradation temperature of NWF-serine decreased slightly and the carbon residue content (13.4%) increased significantly owing to the presence of sodium.

3.2.3 SEM

The micro-morphologies of the NWF samples were characterized using SEM, and the corresponding images are shown in Fig. 3d. The surface of the pristine PE/PP NWF contained rough interwoven fibers with an approximate diameter of $10.1\text{ }\mu\text{m}$. After grafting GMA, the diameter increased to $17.9\text{ }\mu\text{m}$, corresponding to the grafted layer.

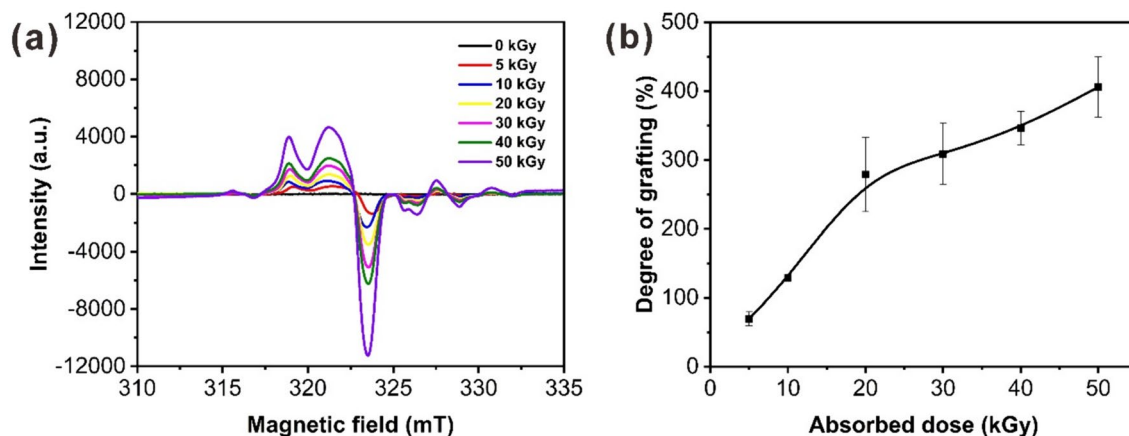


Fig. 2 **a** ESR spectra of PE/PP NWF samples with different absorbed doses, **b** Influence of the absorbed dose on D_g

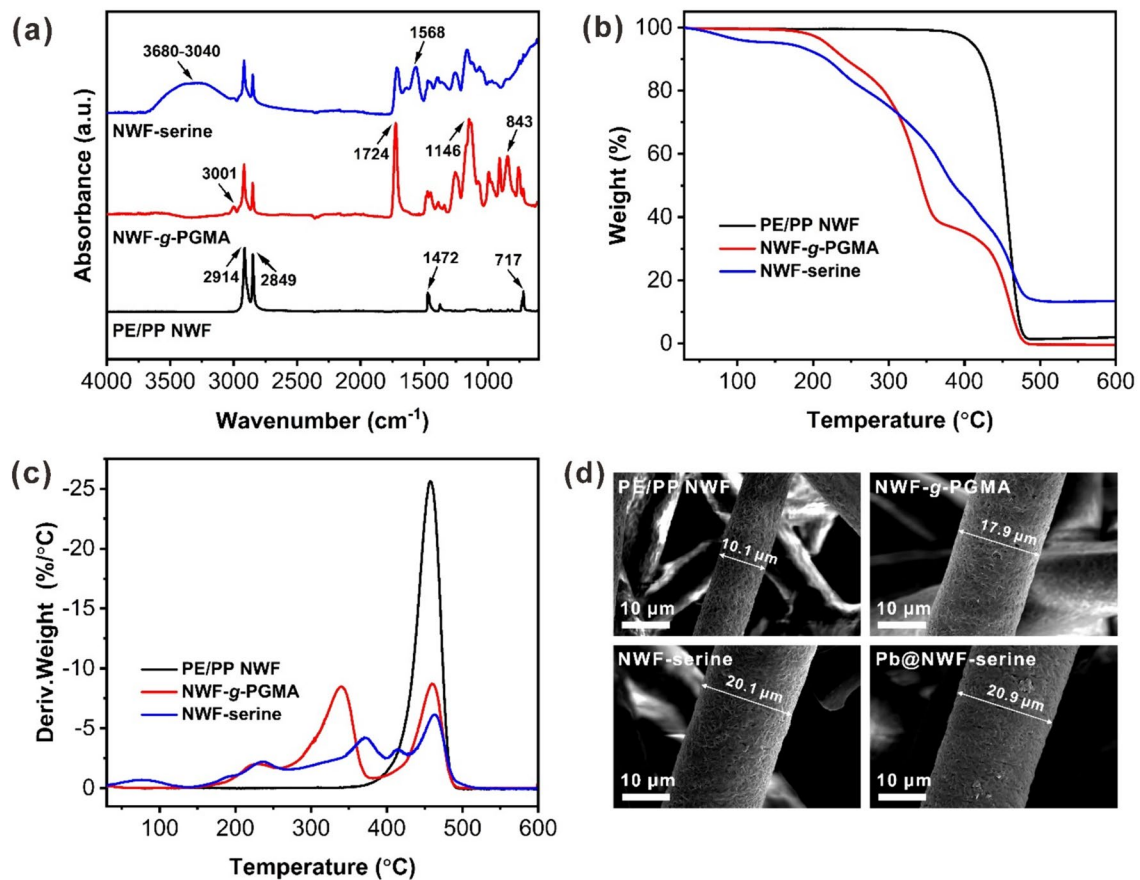


Fig. 3 a FTIR spectra, b TGA curves, c DTG curves, and d SEM images of NWF samples

After modification with L-serine and Pb(II) adsorption, the diameter further increased to 20.1 and 20.9 μm , respectively.

3.3 Adsorption performance characterization

3.3.1 Influence of pH

The pH of the solution significantly influenced the existence form of metal ions and the surface charge of the sorbents. Therefore, the effect of the initial pH on Pb(II) adsorption was evaluated. Adsorption tests were conducted within the pH range of 1–6 to avoid the precipitation of $\text{Pb}(\text{OH})_2$, which occurs at higher pH values. As shown in Fig. 4, within the pH range of 1 (5.0 mg/g) to 3 (11.7 mg/g), Pb(II) uptake remained at a low level. However, at pH 4, Pb(II) uptake sharply increased to 86.4 mg/g, followed by further increases at pH 5 (144.8 mg/g) and 6 (165.4 mg/g). In highly acidic solutions, H^+ ions compete with Pb(II) for active sites on NWF-serine [24]. As the pH increased, the $-\text{COOH}$ groups were converted to $-\text{COO}^-$ groups, exhibiting electrostatic attraction to the positively charged Pb(II) [4]. Additionally, deprotonation of the $-\text{COOH}$ groups stretched the graft chain, promoting better contact with Pb(II) [25]

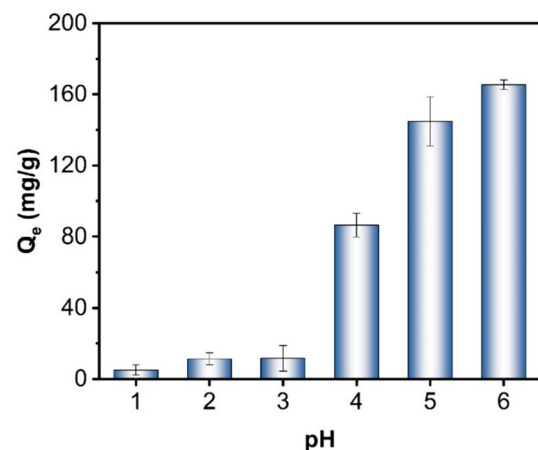
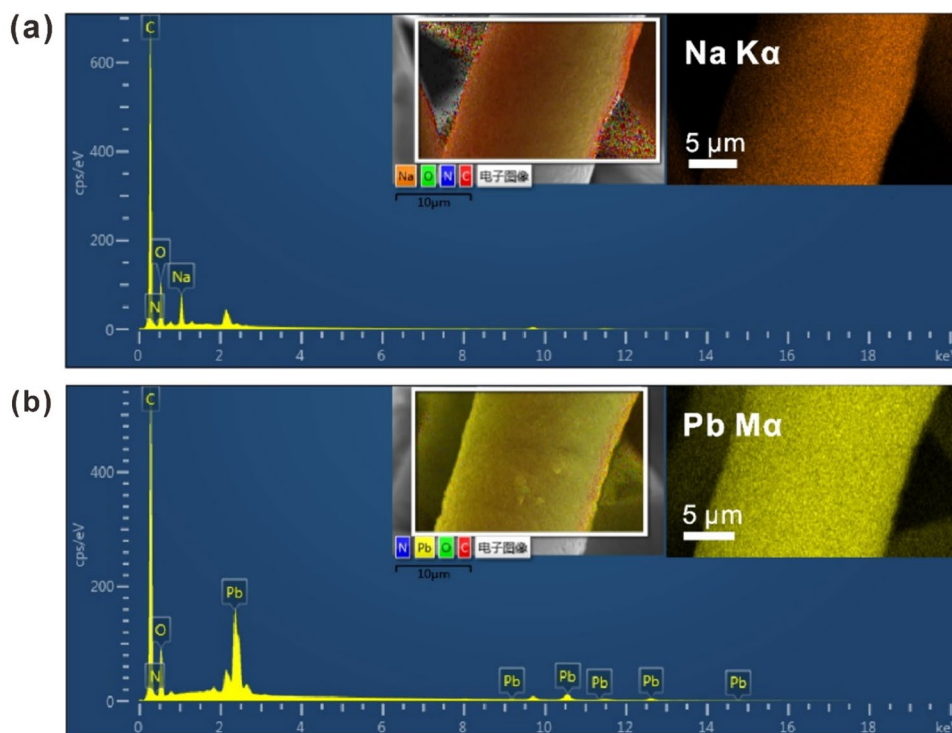


Fig. 4 Influence of solution pH on the Pb(II) adsorption by the NWF-serine. (time, 120 h; Pb(II) concentration, 100 mg/L; sorbent dosage, 0.1 g/L)

To confirm the successful adsorption of Pb(II), EDS analyses were conducted on NWF-serine and Pb@NWF-serine, as presented in Fig. 5. The C, N, O, and Na observed in NWF-serine were attributed to the introduced PGMA chains

Fig. 5 EDS results of **a** NWF-serine and **b** Pb@NWF-serine



and immobilized L-serine molecules. After adsorption, Na disappeared, and the Pb element (20.13 wt%) was detected. Pb(II) was uniformly distributed along the surface of the fibers.

3.3.2 Adsorption kinetics

Adsorption kinetics analysis was conducted to evaluate the adsorption performance of NWF-serine with sorption times in the range of 6–216 h. The influence of temperature was also investigated at 25, 33, and 40 °C, and the results are shown in Fig. 6. With prolonged sorption time, the uptakes of Pb(II) increased significantly within the first 24 h (25 °C, 120.6 mg/g; 33 °C, 144.4 mg/g; 40 °C, 165.4 mg/g), followed by a slow increase until reaching saturation at 216 h (25 °C, 158.0 mg/g; 33 °C, 178.6 mg/g; 40 °C, 201.8 mg/g). To further investigate the adsorption behavior, pseudo-first-order (Eq. 6) and pseudo-second-order (Eq. 7) kinetic models were used to simulate experimental data [26].

$$Q_t = Q_e [1 - \exp(-k_1 t)] \quad (6)$$

$$\frac{1}{Q_e - Q_t} = \frac{1}{Q_e} + k_2 t \quad (7)$$

where Q_t (mg/g) and Q_e (mg/g) are the Pb(II) uptakes at time t and equilibrium, respectively; k_1 (1/h) and k_2 [g/(mg h)] are the rate constants of the two kinetic models. The fitting results and parameters are summarized in Fig. 6 and

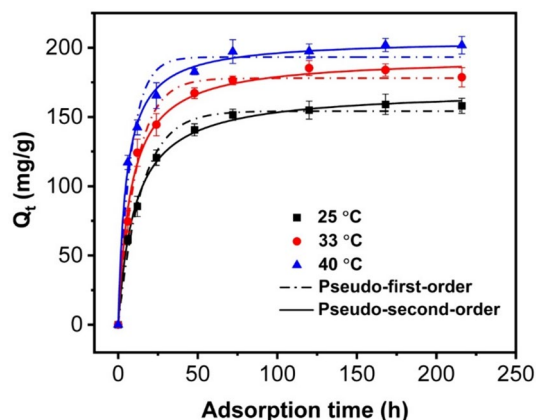
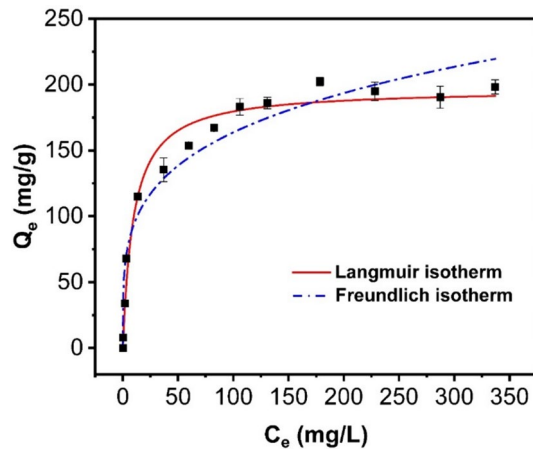


Fig. 6 Influence of sorption time on Pb(II) adsorption and adsorption kinetic models fitting (pH, 6; sorbent dosage, 0.1 g/L; initial concentration, 100 mg/L)

Table 1. Compared with the correlation coefficient of R_1^2 (25 °C: 0.992; 33 °C: 0.988; 40 °C: 0.974 mg/g), the larger R_2^2 (25 °C: 0.997; 33 °C: 0.993; 40 °C: 0.997) indicates that the Pb(II) adsorption process on the NWF-serine conforms to the pseudo-second-order model. The adsorption of Pb(II) occurred through chemical adsorption, involving the exchange or sharing of electrons between NWF-serine and Pb(II) [27]. Furthermore, Pb(II) adsorption on NWF-serine is an endothermic process due to the increase in temperature, which is conducive to the increase in Pb(II) uptakes [28].

Table 1 Fitting parameters of kinetic models

T (°C)	Pseudo-first-order model			Pseudo-second-order model		
	k_1 (1/h)	Q_e (mg/g)	R_1^2	k_2 [g/(mg·h)]	Q_e (mg/g)	R_2^2
25	0.068	154.2	0.992	0.00056	169.6	0.997
33	0.088	178.0	0.988	0.00065	193.1	0.993
40	0.125	193.3	0.974	0.00097	205.9	0.997

**Fig. 7** Adsorption isotherm curve and isotherm models fitting of Pb(II) adsorption by the NWF-serine (time, 120 h; pH, 6; sorbent dosage, 0.1 g/L)

3.3.3 Adsorption isotherms

The adsorption isotherm analysis was conducted by varying the initial Pb(II) concentration from 1 to 350 mg/L. As shown in Fig. 7, a sharp initial slope was observed for equilibrium concentrations between 0.2 mg/L (Q_e , 7.9 mg/g) and 13.5 mg/L (Q_e , 114.9 mg/g) owing to

the increasing driving force generated by the concentration gradient. As the initial concentration continued to increase, the Pb(II) uptakes gradually increased and reached adsorption saturation at a C_e of 337 mg/L (Q_e , 198.1 mg/g). Compared with various previously reported fiber and nonwoven fabric sorbents (Table 2), NWF-serine has a good adsorption capacity. Further analysis of the adsorption process was conducted using Langmuir and Freundlich isotherm models described by Eqs. (8) and (9), respectively [29, 30].

$$Q_e = Q_m \frac{K_L C_e}{1 + K_L C_e} \quad (8)$$

$$Q_e = K_F C_e^{1/n} \quad (9)$$

where C_e (mg/L) and Q_e (mg/g) are the Pb(II) concentration and uptake, respectively, at equilibrium; Q_m (mg/g) is the maximum Pb(II) uptake. The related parameters, K_L (adsorption equilibrium constant), $1/n$ (constant representing the adsorption intensity), K_F (constant describing the adsorption capacity), and R^2 (correlation coefficient), are listed in Table 3. The larger value of R_3^2 (0.970) compared to R_4^2 (0.950) indicates that the Langmuir model describes the Pb(II) adsorption process more accurately. Thus, Pb(II) adsorption occurs via monolayer sorption with uniform surface forces [31]. Moreover, the theoretical adsorption

Table 2 Comparison of the Pb(II) adsorption capacity of NWF-serine with fiber or fabric-based sorbents reported in the literature

Sorbent	Q_e (mg/g)	pH	Reference
Amidoxime-functionalized polypropylene fiber	45.64	5	[32]
Hydrophilic kapok fiber	94.41 ± 7.56	6	[33]
Amine functionalized water hyacinth fiber	100	6	[34]
Activated carbon fibers modified by L-cysteine	179.53	6	[35]
Nonwoven-based double-network composite hydrogel	233.12	5	[36]
UiO-66-NH ₂ functionalized polyacrylamide-grafted nonwoven fabric	711.99	5	[37]
NWF-serine	198.1	6	This work

Table 3 Fitting parameters of isotherm models

T (°C)	Langmuir model			Freundlich model		
	Q_m (mg/g)	K_L (L/mg)	R_3^2	K_F (L ^{1/n} mg ^{(1-1/n)/g})	$1/n$	R_4^2
25	196.8	0.10	0.970	53.71	0.242	0.950

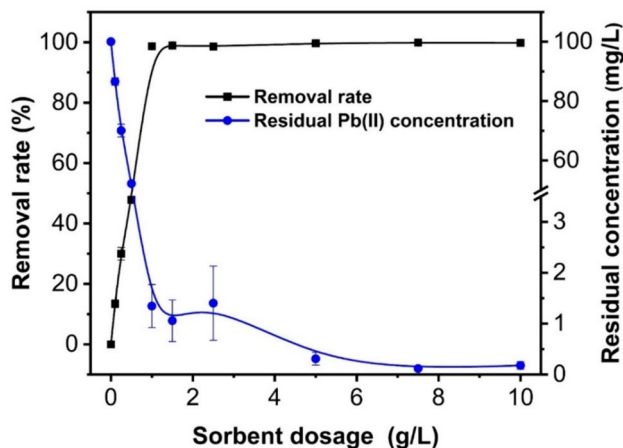


Fig. 8 Influence of sorbent dosage on the adsorption (time, 120 h; initial concentration, 100 mg/L; pH, 6)

capacity predicted using the Langmuir model (196.8 mg/g) was consistent with the experimental adsorption capacity (198.1 mg/g).

3.3.4 Influence of sorbent dosage

To define the optimal sorbent dosage, the effect of different amounts of NWF-serine, in the range of 0.1–10 g/L, on the Pb(II) removal rate was investigated. Figure 8 shows the influence of sorbent dosage on the removal rate and residual concentration of Pb(II). An increase in sorbent dosage provided more binding sites. Thus, the removal ratio rapidly increased to 98.7% at 1.0 g/L, followed by a smooth increase to 99.8% at 10 g/L (residual concentration of 0.18 mg/L). Further adsorption is challenging because equilibrium is gradually reached.

3.3.5 Reusability performance

Five adsorption and desorption cycles were conducted to evaluate the reusability of NWF-serine. Following each Pb(II) adsorption test (initial concentration: 100 mg/L; pH: 6; time: 120 h; sorbent dosage: 0.1 g/L), the NWF-serine was subjected to desorption by immersion in 0.5 mol/L HCl solution for 24 h. Subsequently, sorbent regeneration was achieved by immersion in 0.5 mol/L NaOH solution for 1 h, followed by rinsing with distilled water for 1 h. The results in Fig. 9 show a slight decrease in the Pb(II) uptake as the adsorption cycles progressed. Even after five cycles, NWF-serine retained 86% of its initial adsorption capacity, indicating good reusability.

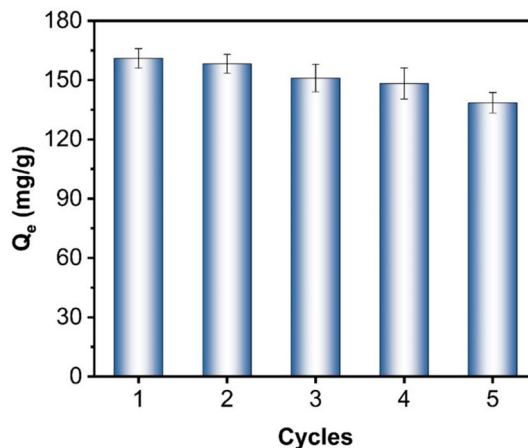


Fig. 9 Reusability performance of NWF-serine

3.3.6 Landfill leachate adsorption

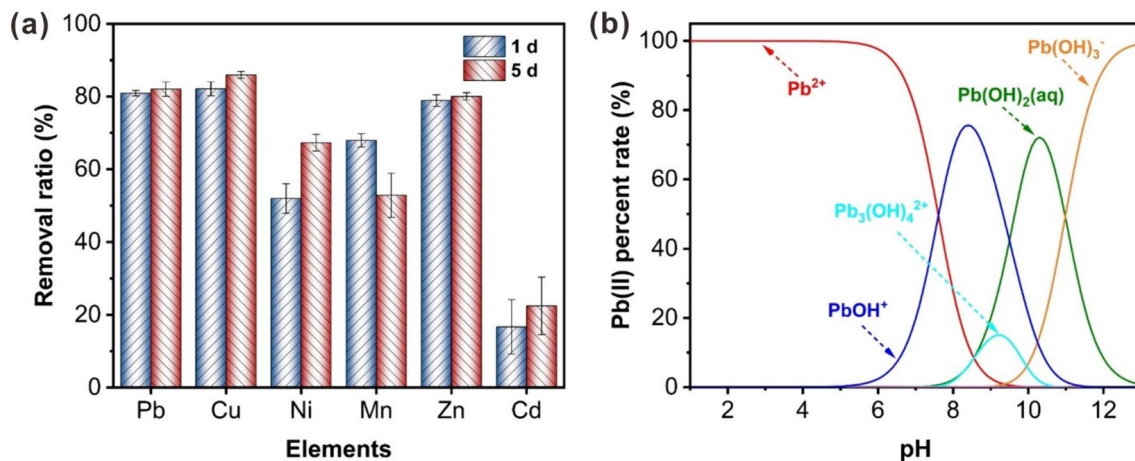
Compared to Pb(II) solutions prepared in the laboratory, wastewater typically contains more complex components. In this study, landfill leachate was used to examine the adsorption performance of the NWF-serine sorbent. The landfill leachate was pre-filtered using a microporous filter membrane to remove insoluble impurities. The pH of the landfill leachate was measured as 7.9. Before determining the concentration, the landfill leachate was subjected to microwave digestion. Table 4 presents the typical heavy-metal ion concentrations in landfill leachate before and after adsorption. After adsorption for 5d, the Pb concentration was reduced to 1.73 mg/L, with the removal rate reaching 82.1%. Moreover, the concentrations of metal ions with high initial concentrations, such as Cd (52.37 mg/L) and Zn (95.06 mg/L), were reduced to 40.61 and 18.99 mg/L, respectively. This indicates that NWF-serine is promising for treating sewage containing heavy-metal ions. The primary species of heavy-metal ions at pH 7.9 were calculated using Visual MINTEQ 3.1 [38] and are detailed in Fig. 10b and Table 5. All metal ions except Pb (PbOH⁺: 64.3%; Pb²⁺: 32.8%) primarily exist as divalent cations, indicating that charge is not the primary factor affecting the difference in removal rates. Notably, heavy-metal ions may exist as complexes with organic matter in landfill leachate [39], thereby interfering with adsorption. However, this aspect requires further investigation.

3.3.7 Mechanism speculation

The adsorption mechanisms of Pb(II) by NWF-serine was investigated via XPS and EXAFS analyses. The XPS spectrum of NWF-serine (Fig. 11a) showed peaks corresponding to C 1s (285 eV), N 1s (399 eV), O 1s (532 eV), and Na 1s (1072 eV). After adsorption, the Na 1s peak disappeared,

Table 4 Composition of landfill leachate before and after adsorption

Adsorption time (d)	Pb (mg/L)	Cu (mg/L)	Ni (mg/L)	Mn (mg/L)	Zn (mg/L)	Cd (mg/L)
0	9.64	11.81	0.52	1.06	95.06	52.37
1	1.84	2.11	0.25	0.34	20.05	43.64
5	1.73	1.66	0.17	0.50	18.99	40.61

**Fig. 10** **a** Removal ratio of metal ions in landfill leachate (sorbent dosage, 5 g/L), **b** Species distribution of Pb at different pH (the data was obtained from Visual MINTEQ 3.1, Pb concentration setting, 10 mg/L; temperature, 25 °C)**Table 5** Primary metal ion species in pH 7.9

	Pb	Cu	Ni	Mn	Zn	Cd
Concentration setting (mg/L)	10	10	1	1	100	50
Primary species	PbOH ⁺	Cu ₃ (OH) ₄ ²⁺	Ni ²⁺	Mn ²⁺	Zn ²⁺	Cd ²⁺

and two Pb 4*f* peaks (139 and 144 eV) emerged in the spectrum of Pb@NWF-serine, which was consistent with the EDS results. The Pb 4*f* high-resolution spectrum (Fig. 11b) exhibited double peaks of Pb 4*f*_{7/2} (138.8 eV) and Pb 4*f*_{5/2} (143.7 eV), indicating that Pb ions were absorbed in bivalent forms [40]. High-resolution O 1*s* and N 1*s* spectra are shown in Fig. 11d, e, respectively. The N 1*s* peak can be divided into two distinct peaks: R₂NH (399.3 eV) and R₂NH₂⁺ (401.6 eV). After adsorption, new peaks assigned to O–Pb (530.8 eV) [41] and N–Pb (399.8 eV) emerged, along with a decrease in the peak area of O=C–O, indicating the potential involvement of amino and carboxyl groups in the coordination process. The EXAFS analysis results further illustrated the local bond lengths and coordination structures of Pb. Figure 11c shows a well-fitted Fourier transform in the *R* space. The local structural parameters for Pb@NWF-serine are listed in Table 6, where coordination numbers for Pb–O and Pb–N are 2.0 and 2.2, respectively. Figure 11f shows the

proposed Pb coordination structure. Notably, five-membered chelate rings were preferred by Pb(II) over other sizes [42], which is consistent with the structure we speculated.

N, coordination numbers; *R*, the interatomic distance; σ^2 , Debye–Waller factor; *R*_{factor}, goodness of fit; ΔE_0 , the inner potential correction.

4 Conclusion

A novel NWF-serine sorbent was successfully synthesized to efficiently remove Pb(II) from aqueous solutions and landfill leachate. The sorbent was characterized by FTIR spectroscopy, TGA, SEM, EDS, XPS, and EXAFS analysis. The optimal absorbed dose for the sorbent synthesis was determined to be 20 kGy. The most effective pH for Pb(II) adsorption was 6 in the pH range of 1–6. The increase in Pb(II) uptake with increasing temperature indicated that the

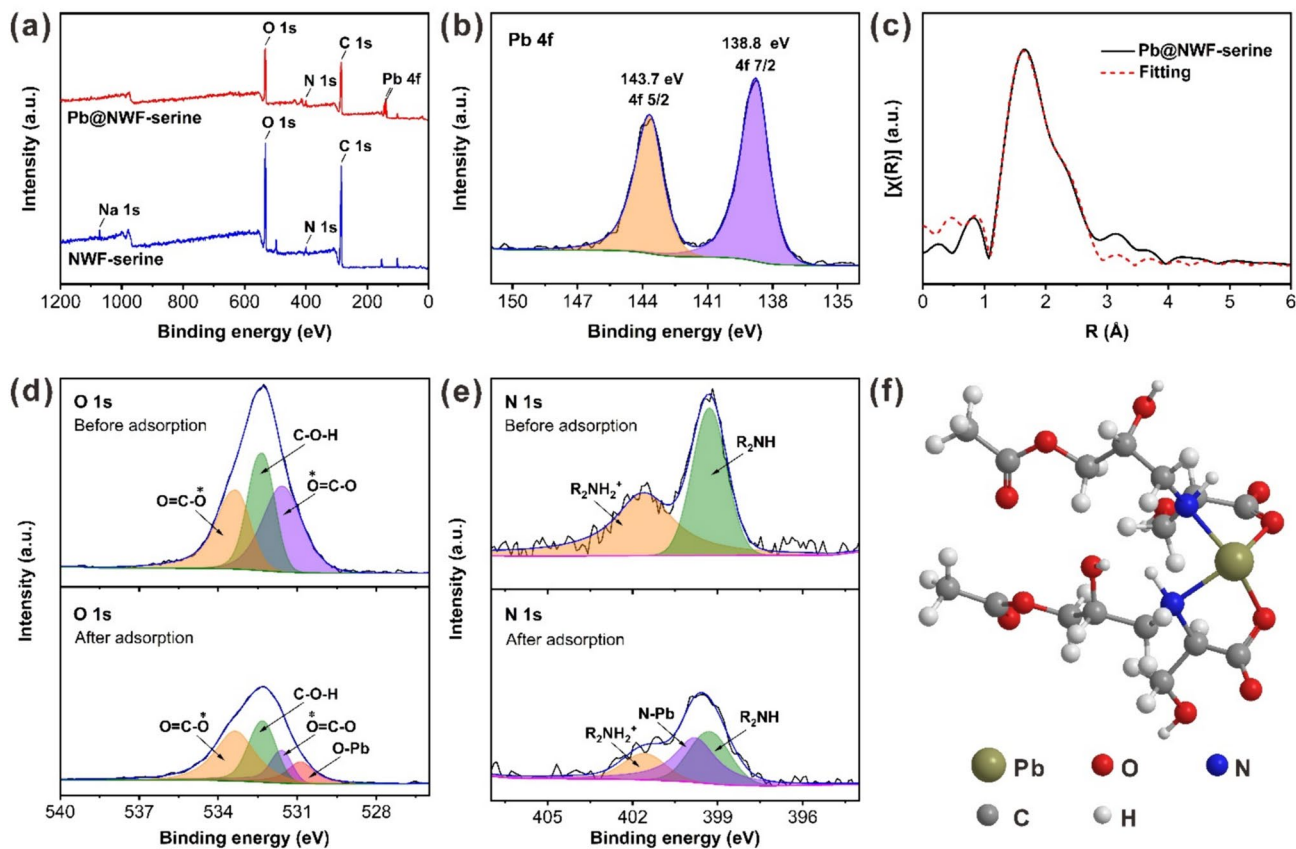


Fig. 11 **a** XPS spectra of NWF-serine and Pb@NWF-serine, **b** XPS high-resolution spectrum of Pb 4f, **c** EXAFS fitting curves of Pb@NWF-serine; XPS high-resolution spectra of **d** O 1s and **e** N 1s; **f** The coordination structure of Pb

adsorption process was endothermic. The investigation of the adsorption kinetics and isotherms confirmed that Pb(II) adsorption by NWF-serine followed a monolayer chemisorption process, with a saturated adsorption capacity of 198.1 mg/g. The Pb(II) uptake was maintained at 86% of its initial value after five cycles. Notably, the Pb(II) removal rates from the aqueous solution and landfill leachate were 99.8% and 82.1%, respectively. XPS and EXAFS structure analyses indicated the involvement of carboxyl and amino groups in the coordination of Pb ions. These results demonstrated the potential of NWF-serine for removing Pb(II) from contaminated wastewater.

Author contributions All authors contributed to the study conception and design. Material preparation, data collection and analysis were

performed by Xin-Xin Feng, Cheng Li, Xuan-Zhi Mao, Wan-Ning Ren, Rong Li and Guo-Zhong Wu. The first draft of the manuscript was written by Xin-Xin Feng and all authors commented on previous versions of the manuscript. All authors read and approved the final manuscript.

Data availability The data that support the findings of this study are openly available in Science Data Bank at <https://cstr.cn/31253.11.sciencedb.j00186.00485> and <https://www.doi.org/10.57760/sciencedb.j00186.00485>.

Declarations

Conflict of interest The authors declare that they have no competing interests.

References

1. K.Y. Foo, B.H. Hameed, An overview of landfill leachate treatment via activated carbon adsorption process. *J. Hazard. Mater.* **171**, 54–60 (2009). <https://doi.org/10.1016/j.jhazmat.2009.06.038>
2. M.A.M. Reshadi, A. Bazargan, G. McKay, A review of the application of adsorbents for landfill leachate treatment: focus on magnetic adsorption. *Sci. Total. Environ.* **731**, 138863 (2020). <https://doi.org/10.1016/j.scitotenv.2020.138863>
3. M.L. Sall, A.K.D. Diaw, D. Gningue-Sall et al., Toxic heavy metals: impact on the environment and human health, and treatment

Table 6 Local structure parameters at the Pb L_{3} -edge for Pb@NWF-serine samples

Shell	N	R (Å)	σ^2	R_{factor}	ΔE_0 (eV)
Pb–O	2.0 ± 0.2	2.33 ± 0.001	0.007 ± 0.0001	0.005	–9.07
Pb–N	2.2 ± 0.3	2.54 ± 0.002	0.01 ± 0.0001	0.005	9.15

- with conducting organic polymers, a review. *Environ. Sci. Pollut. Res.* **27**, 29927–29942 (2020). <https://doi.org/10.1007/s11356-020-09354-3>
4. T. Depci, A.R. Kul, Y. Önal, Competitive adsorption of lead and zinc from aqueous solution on activated carbon prepared from Van apple pulp: study in single- and multi-solute systems. *Chem. Eng. J.* **200–202**, 224–236 (2012). <https://doi.org/10.1016/j.cej.2012.06.077>
 5. N. Corda, M.S. Kini, Recent studies in adsorption of Pb(II), Zn(II) and Co(II) using conventional and modified materials: a review. *Sep. Sci. Technol.* **55**, 2679–2698 (2020). <https://doi.org/10.1080/01496395.2019.1652651>
 6. Ministry of Ecology and Environment of the People's Republic of China. Standard for pollution control on the landfill site of municipal solid waste (GB 16889-2008). https://www.mee.gov.cn/ywgz/fgbz/bz/bzwb/gthw/gtfwwrkzbx/200804/t20080414_121136.shtml. Accessed 3 June 2023
 7. F. Zhu, H.J. Lu, Y.H. Lu, Effective solid phase extraction for the enrichment of p-nitrophenol in water using microwave-assisted synthesized fly ash@p-nitrophenol surface molecular imprinted polymer. *J. Mater. Sci.* **58**, 4399–4415 (2023). <https://doi.org/10.1007/s10853-023-08302-z>
 8. N. Li, H.J. Lu, Y.K. Liang et al., Microwave-assisted magnetic Cu(II)-imprinted-polymer based on double functional monomers for selective removal of Cu(II) from wastewater. *J. Water Chem. Technol.* **44**, 431–439 (2022). <https://doi.org/10.3103/S1063455X2206008X>
 9. F. Zhu, L.W. Li, N. Li et al., Selective solid phase extraction and preconcentration of Cd(II) in the solution using microwave-assisted inverse emulsion-suspension Cd(II) ion imprinted polymer. *Microchem. J.* **164**, 106060 (2021). <https://doi.org/10.1016/j.microc.2021.106060>
 10. E.A. Gendy, J. Ifthikar, J. Ali et al., Removal of heavy metals by covalent organic frameworks (COFs): a review on its mechanism and adsorption properties. *J. Environ. Chem. Eng.* **9**, 105687 (2021). <https://doi.org/10.1016/j.jece.2021.105687>
 11. R. Shrestha, S. Ban, S. Devkota et al., Technological trends in heavy metals removal from industrial wastewater: a review. *J. Environ. Chem. Eng.* **9**, 105688 (2021). <https://doi.org/10.1016/j.jece.2021.105688>
 12. Q. Jiang, W.L. Xie, S.Y. Han et al., Enhanced adsorption of Pb(II) onto modified hydrochar by polyethyleneimine or H₃PO₄: an analysis of surface property and interface mechanism. *Colloid Surface A* **583**, 123962 (2019). <https://doi.org/10.1016/j.colsurfa.2019.123962>
 13. P. Bhunia, S. Chatterjee, P. Rudra et al., Chelating polyacrylonitrile beads for removal of lead and cadmium from wastewater. *Sep. Purif. Technol.* **193**, 202–213 (2018). <https://doi.org/10.1016/j.seppur.2017.11.001>
 14. R. Li, Y.N. Li, M.J. Zhang et al., Phosphate-based ultrahigh molecular weight polyethylene fibers for efficient removal of uranium from carbonate solution containing fluoride ions. *Molecules* **23**, 1245 (2018). <https://doi.org/10.3390/molecules23061245>
 15. L. Hakim, A. Sabarudin, M. Oshima et al., Synthesis of novel chitosan resin derivatized with serine diacetic acid moiety and its application to on-line collection/concentration of trace elements and their determination using inductively coupled plasma-atomic emission spectrometry. *Anal. Chim. Acta* **588**, 73–81 (2007). <https://doi.org/10.1016/j.aca.2007.01.066>
 16. K. Oshita, M. Oshima, Y.H. Gao et al., Synthesis of novel chitosan resin derivatized with serine moiety for the column collection/concentration of uranium and the determination of uranium by ICP-MS. *Anal. Chim. Acta* **480**, 239–249 (2003). [https://doi.org/10.1016/S0003-2670\(03\)00020-5](https://doi.org/10.1016/S0003-2670(03)00020-5)
 17. N. Belachew, D. Rama Devi, K. Basavaiah, Green synthesis and characterisation of L-Serine capped magnetite nanoparticles for removal of Rhodamine B from contaminated water. *J. Exp. Nanosci.* **12**, 114–128 (2017). <https://doi.org/10.1080/17458080.2017.1279354>
 18. Ş Yılmaz, A. Zengin, T. Şahan, A novel material poly (N-acryloyl-L-serine)-brush grafted kaolin for efficient elimination of malachite green dye from aqueous environments. *Colloids Surf. A* **601**, 125041 (2020). <https://doi.org/10.1016/j.colsurfa.2020.125041>
 19. N. Seko, M. Tamada, F. Yoshii, Current status of adsorbent for metal ions with radiation grafting and crosslinking techniques. *Nucl. Instrum. Meth. B.* **236**, 21–29 (2005). <https://doi.org/10.1016/j.nimb.2005.03.244>
 20. B. Ravel, M. Newville, ATHENA, ARTEMIS, HEPHAESTUS: data analysis for X-ray absorption spectroscopy using IFEFFIT. *J. Synchrotron Radiat.* **12**, 537–541 (2005). <https://doi.org/10.1107/S0909049505012719>
 21. P. Bracco, L. Costa, M.P. Luda et al., A review of experimental studies of the role of free-radicals in polyethylene oxidation. *Polym. Degrad. Stab.* **155**, 67–83 (2018). <https://doi.org/10.1016/j.polymdegradstab.2018.07.011>
 22. Y. Ma, M. Yu, L.F. Li et al., Reversible addition-fragmentation chain transfer graft polymerization of acrylonitrile onto PE/PET composite fiber initiated by gamma-irradiation. *Nucl. Sci. Tech.* **26**, 020301 (2015). <https://doi.org/10.13538/j.1001-8042/nst.26.20301>
 23. M.X. Zhang, J.C. Chen, M.L. Wang et al., Electron beam-induced preparation of AIE non-woven fabric with excellent fluorescence durability. *Appl. Surf. Sci.* **541**, 148382 (2021). <https://doi.org/10.1016/j.apsusc.2020.148382>
 24. M.X. Zhang, Q.H. Gao, C.G. Yang et al., Preparation of amidoxime-based nylon-66 fibers for removing uranium from low-concentration aqueous solutions and simulated nuclear industry effluents. *Ind. Eng. Chem. Res.* **55**, 10523–10532 (2016). <https://doi.org/10.1021/acs.iecr.6b02652>
 25. X. Hao, C. Xian, H. Wang et al., Preparation of hydroxoxime group-modified ultra-high molecular weight polyethylene fiber adsorbent by radiation-induced graft polymerization and its application to heavy metal ions removal. *J. Radiat. Res. Radiat. Process.* **41**, 020201 (2023). <https://doi.org/10.11889/j.1000-3436.2022-0088>
 26. L.L. Zang, J. Ma, D.W. Lv et al., A core-shell fiber-constructed pH-responsive nanofibrous hydrogel membrane for efficient oil/water separation. *J. Mater. Chem. A* **5**, 19398–19405 (2017). <https://doi.org/10.1039/c7ta05148d>
 27. Y.S. Ho, G. McKay, Pseudo-second order model for sorption processes. *Process Biochem.* **34**, 451–465 (1999). [https://doi.org/10.1016/S0032-9592\(98\)00112-5](https://doi.org/10.1016/S0032-9592(98)00112-5)
 28. C.Y. Xie, S.P. Jing, Y. Wang et al., Adsorption of uranium(VI) onto amidoxime-functionalized ultra-high molecular weight polyethylene fibers from aqueous solution. *Nucl. Sci. Tech.* **28**, 94 (2017). <https://doi.org/10.1007/s41365-017-0251-6>
 29. A.S. Özcan, Ö. Gök, A. Özcan, Adsorption of lead(II) ions onto 8-hydroxy quinoline-immobilized bentonite. *J. Hazard. Mater.* **161**, 499–509 (2009). <https://doi.org/10.1016/j.jhazmat.2008.04.002>
 30. I. Langmuir, The constitution and fundamental properties of solids and liquids. *J. Frankl. Inst.* **183**, 102–105 (1917). <https://doi.org/10.1021/ja02268a002>
 31. D.G. Kinniburgh, General purpose adsorption isotherms. *Environ. Sci. Technol.* **20**, 895–904 (1986). <https://doi.org/10.1021/es00151a008>
 32. H.M. Du, Y.J. Xie, H.N. Zhang et al., Oxadiazole-functionalized fibers for selective adsorption of Hg²⁺. *Ind. Eng. Chem. Res.* **59**, 13333–13342 (2020). <https://doi.org/10.1021/acs.iecr.0c01562>
 33. D.Z. Zhao, Z. Wang, S. Lu et al., An amidoxime-functionalized polypropylene fiber: competitive removal of Cu(II), Pb(II) and Zn(II) from wastewater and subsequent sequestration in cement

- mortar. *J. Clean. Prod.* **274**, 123049 (2020). <https://doi.org/10.1016/j.jclepro.2020.123049>
34. D.F. Wang, D. Kim, C.H. Shin et al., Removal of lead(II) from aqueous stream by hydrophilic modified kapok fiber using the Fenton reaction. *Environ. Earth Sci.* **77**, 653 (2018). <https://doi.org/10.1007/s12665-018-7824-5>
35. J.F. Madrid, G.M. Nuesca, L.V. Abad, Amine functionalized radiation-induced grafted water hyacinth fibers for Pb²⁺, Cu²⁺ and Cr³⁺ uptake. *Radiat. Phys. Chem.* **97**, 246–252 (2014). <https://doi.org/10.1016/j.radphyschem.2013.12.009>
36. L.K. Zhu, Y.Y. Yao, D.Z. Chen et al., The effective removal of Pb²⁺ by activated carbon fibers modified by l-cysteine: exploration of kinetics, thermodynamics and mechanism. *RSC Adv.* **12**, 20062–20073 (2022). <https://doi.org/10.1039/D2RA01521H>
37. T.T. Li, Z.K. Wang, H.T. Ren et al., Recyclable and degradable nonwoven-based double-network composite hydrogel adsorbent for efficient removal of Pb(II) and Ni(II) from aqueous solution. *Sci. Total. Environ.* **758**, 143640 (2021). <https://doi.org/10.1016/j.scitotenv.2020.143640>
38. F. Zhao, C.H. Su, W.X. Yang et al., In-situ growth of UiO-66-NH₂ onto polyacrylamide-grafted nonwoven fabric for highly efficient Pb(II) removal. *Appl. Surf. Sci.* **527**, 146862 (2020). <https://doi.org/10.1016/j.apsusc.2020.146862>
39. J. P. Gustafsson. Visual MINTEQ 3.1. (Stockholm, Sweden, 2020), <https://vminteq.com/download/>. Accessed 11 Apr 2024
40. T.H. Christensen, P. Kjeldsen, P.L. Bjerg et al., Biogeochemistry of landfill leachate plumes. *Appl. Geochem.* **16**, 659–718 (2001). [https://doi.org/10.1016/S0883-2927\(00\)00082-2](https://doi.org/10.1016/S0883-2927(00)00082-2)
41. J.X. Li, S.Y. Chen, G.D. Sheng et al., Effect of surfactants on Pb(II) adsorption from aqueous solutions using oxidized multiwall carbon nanotubes. *Chem. Eng. J.* **166**, 551–558 (2011). <https://doi.org/10.1016/j.cej.2010.11.018>
42. X.D. Zhao, Y.X. Wang, Y.L. Li et al., Synergy effect of pore structure and amount of carboxyl site for effective removal of Pb²⁺ in metal-organic frameworks. *J. Chem. Eng. Data* **64**, 2728–2735 (2019). <https://doi.org/10.1021/acs.jced.9b00130>
43. E.S. Claudio, H.A. Godwin, J.S. Magyar, Fundamental coordination chemistry, environmental chemistry, and biochemistry of lead (II), in *Progress in inorganic chemistry*, vol. 51, (John Wiley & Sons, Inc., Canada, 2002), p.73

Springer Nature or its licensor (e.g. a society or other partner) holds exclusive rights to this article under a publishing agreement with the author(s) or other rightsholder(s); author self-archiving of the accepted manuscript version of this article is solely governed by the terms of such publishing agreement and applicable law.